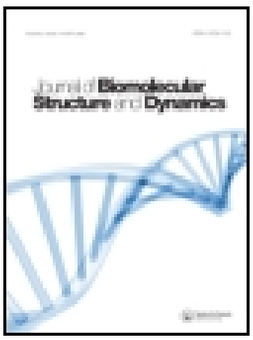

Taylor & Francis
Taylor & Francis Group

Journal of Biomolecular Structure and Dynamics

ISSN: (Print) (Online) Journal homepage: https://www.tandfonline.com/loi/tbsd20

Shedding light on the bimolecular interactions of Cafaminol and human serum albumin: spectroscopic characterization and in-silico investigation

Negar Parvizi , Delara Mohammad-Aghaie , Mohammad Navid Soltani Rad , Somayeh Behrouz & Mohamad Mehdi Alavianmehr

To cite this article: Negar Parvizi , Delara Mohammad-Aghaie , Mohammad Navid Soltani Rad , Somayeh Behrouz & Mohamad Mehdi Alavianmehr (2021): Shedding light on the bimolecular interactions of Cafaminol and human serum albumin: spectroscopic characterization and in-silico investigation, Journal of Biomolecular Structure and Dynamics, DOI: 10.1080/07391102.2020.1863262

To link to this article: https://doi.org/10.1080/07391102.2020.1863262

JOURNAL OF BIOMOLECULAR STRUCTURE AND DYNAMICS
https://doi.org/10.1080/07391102.2020.1863262

Shedding light on the bimolecular interactions of Cafaminol and human serum albumin: spectroscopic characterization and in-silico investigation

Negar Parvizi, Delara Mohammad-Aghaie, Mohammad Navid Soltani Rad, Somayeh Behrouz and Mohamad Mehdi Alavianmehr

Department of Chemistry, Shiraz University of Technology, Shiraz, Iran

Communicated by Ramaswamy H. Sarma

ABSTRACT

Cafaminol, also known as methylcoffanolamine, is a vasoconstrictor and anticatarrhal of the methylxanthine family, which is used as a nasal decongestant. This study aimed to investigate the interaction mechanisms of human serum albumin (HSA) with Cafaminol, through several spectroscopic (fluorescence quenching, UV-visible absorption, and circular dichroism (CD) spectroscopies) and molecular modeling techniques. Stern-Volmer plots were employed to specify the fluorescence quenching mechanism, while the simulation methods were utilized to deduce the approximate binding position of Cafaminol on HSA. On the other hand, thermodynamic parameters, enthalpy and entropy changes, were determined to be, respectively, -105.88 (kJ mol^{-1}) and -282.34 (J mol^{-1} K^{-1}), using the Van't Hoff equation and analyzed later to specify the main acting forces between Cafaminol and HSA. Overall results revealed the binding of Cafaminol to the site I of HSA, as a result of an enthalpy-driven process, mainly through the van der Waals and hydrogen bonding interactions. Static quenching mechanism was found to be responsible for the fluorescence quenching of HSA in the Cafaminol presence, while the number of binding sites and apparent binding constant were measured accordingly. Docking results proposed that Cafaminol and HSA interact with a binding free energy (ΔG) of -6.5 kcal mol^{-1}

ARTICLE HISTORY
Received 11 August 2020
Accepted 8 December 2020

KEYWORDS
Human serumal bumin; fluorescence spectroscopy; molecular dynamics simulation; Cafaminol

1. Introduction

Human Serum Albumin (HSA, shown in Figure 1) has a fundamental role in the transport and deposition of many endogenous and exogenous substances in blood. It is a single-chain protein of 585 aminoacids and a molecular mass of 66.5 kDa, with a usual concentration of around 42 mg/ml (Peters, 1995). This heart shaped molecule with approximate dimensions of $80 \times 80 \times 30$ Å, has three specific homologous α-helical domains, I, II and III, while each of them are divided into sub-domains, A and B (Peters, 1995; Sugio et al., 1999).

Various small molecules can chemically bound to HSA in sites I (the Warfarine binding site), II (the Benzodiazepine binding site) and III, respectively, located in domains IIA, IIIA and IB, while the last site is relatively novel (Bos et al., 1988, 1988). When encountering with HSA, different drugs may compete for the same binding site.

It is of great importance to determine the interaction of different drugs with HSA, not only to comprehend their transport and metabolism in the body, but also to shed light on their therapeutic effectiveness. It is well known that the binding mechanism has an important pharmacokinetic and pharmacodynamics implications, and the degree of protein binding affects on absorption, distribution and excretion of drugs (Seedher & Bhatia, 2006).

A wide variety of experimental and computational methods have been used for analysis of the interactions between proteins and ligands. Some widely used experimental techniques are X-ray scattering, nuclear magnetic resonance (NMR), Laue X-ray diffraction, single-molecule fluorescence spectroscopy, UV–vis absorption and circular dichroism spectroscopy (Du et al., 2016). On the other hand, molecular dynamics and docking simulations are able to provide microscopic insight into the drug protein interactions.

Alavianmehr et al. (2014) determined the binding properties of N,N',N"-triethylenethiophosphoramide (thioTEPA), with human serum albumin in aqueous solution, at pH 7.4. They employed the UV/vis absorption and fluorescence spectroscopies along with molecular dynamics and docking simulations. ThioTEPA was found to be located at domain I of HSA, resulting in both static and dynamic fluorescence quenching mechanisms, while no significant changes in the local and overall secondary structure, polarity and hydrophobicity of HSA were observed.

Recently, Poursoleiman et al. (2019) studied the interaction of HSA with the two Polymyxins (B & E), which are members of a group of cationic charged cyclic antibiotic

CONTACT Delara Mohammad-Aghaie d_aghaie@sutech.a.ird; delara.a@gmail.com Department of Chemistry, Shiraz University of Technology, Shiraz, 71555-313, Iran

Supplemental data for this article can be accessed online at https://doi.org/10.1080/07391102.2020.1863262

lipopeptides, to get quantitative and qualitative insight into the binding characteristics. Considering the values of thermodynamic parameters revealed that binding interaction was spontaneous and entropy driven. Electrostatic interactions were found to be responsible for binding of polymixins to a moiety of HSA, between domains I and III. The results of both fluorescence anisotropy and Far-UV CD spectroscopies, in agreement with the computational studies, demonstrated minor changes in the HSA conformational structure.

Sohrabi et al. (2018) investigated the mutual interactions of lomefloxacin (LMF) and a calf thymus DNA-histone H1 (ctDNA-H1) complex, through several spectroscopic techniques, along with the viscometry and molecular modeling methods. Analysis of thermodynamic parameters, such as ΔG^0 and ΔS^0, revealed the important role of van der Waals forces and hydrogen bonding, in the LMF binding to ctDNA and the ctDNA-H1 complex. On the other hand, CD spectroscopy confirmed the interaction of LMF with ctDNA and ctDNA-H1, through an outside binding mode, leading to the conformational changes in ctDNA. Both in the absence and presence of H1, the interaction mechanism was found to be static.

In the study of the effects of Nano-Curcumin (Nano-CUR) binding on HSA-HTF (holo transferrin) interactions, Mokaberi et al. (2020) found that Nano-CUR is capable of quenching both proteins with a static mechanism and obtained the binding constants for the formation of binary and ternary complexes. Analysis of thermodynamic parameters revealed the outstanding roles of van der Waals forces and hydrogen bonding interactions, in complex formations. On the other hand, results of the three-dimensional fluorescence spectra indicated the remarkable changes in the structures of HSA, HTF, and (HSA-HTF), in the presence of Nano-CUR, within the binary and ternary systems.

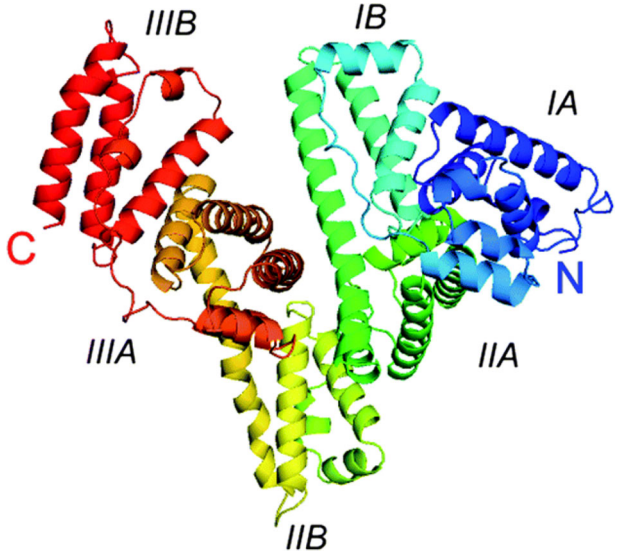

Figure 1. The ribbon model of albumin, derived from X-ray crystallography, where the subdivision of albumin into domains (I, II, III) and subdomains (A and B) is indicated. C and N show the C-terminal and N-terminal ends, respectively.

In continuation of our previous works (Alavianmehr et al., 2014; Keshavarz et al., 2013; Mohammad-Aghaie et al., 2019; Shahsavani et al., 2016), this study aims to elucidate different aspects of Cafaminol-HSA binding interactions, through several spectroscopic and simulation techniques. To the best of our knowledge, there has not been any reported study on the interaction of Cafaminol with the human serum albumin.

Cafaminol [CAS No: 30924-31-3] with the IUPAC name of (8-[(2-ydroxyethyl) (methyl)amino]-1,3,7-trimethyl-3,7-dihydro-1H-purine-2,6-dione), also known as methylcoffanolamine, has been clinically applied as a nasal decongestant and anticatarrhal, since 1974. This drug which is derived from xanthine (a purine base) (Rogowski & Chodynicki, 1985), selectively binds to alpha-1 receptors, causing blood vessels to constrict.

In the present study, binding of Cafaminol to HSA was studied by UV/vis absorption and fluorescence spectroscopies, the fluorescence quenching mechanism was specified and the drug's effect on the protein's secondary structure was explored using the circular dichroism (CD) method. In order to assess the nature of dominant acting forces between HSA and Cafaminol, thermodynamic parameters were analyzed. Furthermore, docking and molecular dynamics simulation methods were employed to get a more solid understanding of the structural features, induced by Cafaminol on HSA, and determine their approximate binding position. These results will be of biological importance in pharmacology as well as clinical medicine.

2. Materials and methods

2.1. Materials

HSA was purchased from sigma Aldrich and used without further purification. Cafaminol was synthesized in our laboratory in two synthetic steps, shown in Figure 2. Primarily, the caffeine was brominated using NBS in DCM/Water (50:50, V/V) solution at room temperature for 5 days, then the obtained 8-bromocaffeine was reacted with N-methylethanol amine, in a neat condition at 170 °C, to obtain the pure Cafaminol as a white solid (mp: 162–164 °C). The physical and spectral data assignments of Cafaminol, comprising ^{1}HNMR, ^{13}CNMR and IR, have been provided as supplementary data.

The stock solution of HSA 30 micro molar (μM) was prepared by dissolving protein in phosphate buffer solution 0.1 M (Na_2HPO_4 and NaH_2PO_4 in pure aqueous medium, with PH = 7.4). Before sample preparation, the protein

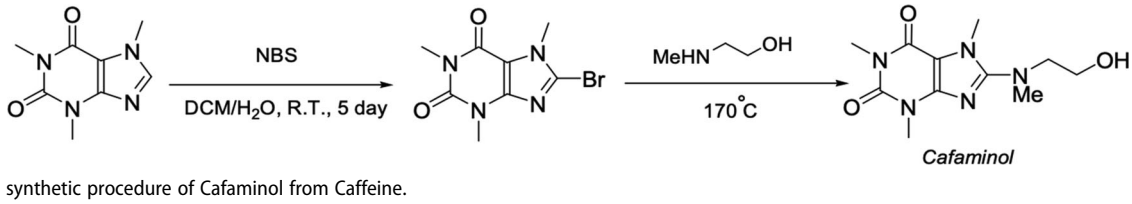

Figure 2. The synthetic procedure of Cafaminol from Caffeine.

concentration was determined spectrophotometrically using an extinction coefficient of 42,000 $M^{-1}cm^{-1}$, at 280 nm (Śpiewak et al., 2015). The Cafaminol working solutions were prepared by dissolving appropriate amounts of Cafaminol in the same buffer. All solutions were stored at 0–4 °C in the dark for a week. Doubly distilled water was used throughout all over experiments.

2.2. Methods

2.2.1. Fluorescence spectroscopy

Fluorescence quenching occurs due to the decrease in the quantum yield of fluorophore, induced by the quencher molecule. The inherent fluorescence of HSA comes mainly from tryptophan-214 and is very sensitive to the environment, around this residue (Lakowicz, 2013).

Here, Cafaminol acts as a quencher for HSA molecule. Fluorescence quenching is classified into dynamic and static quenching. These two mechanisms are distinguished, based on their response to the temperature. To examine the mechanism of Cafaminol induced quenching, the Stern-Volmer equation was employed.

Fluorescence spectra and intensities were measured with carry-Eclipse spectrophotometer (Varian model-Australia) equipped with a thermostat bath and 1-cm quartz cell. Excitation and emission bandwidths were set at 5 and 10 nm, respectively.

The steady-state fluorescence emission spectra of HSA were measured in the 300–450 nm range, at 289, 296, 303 and 310 K, with the wavelength of 295 nm. In each temperature, a 1 ml portion of 10 μmol L^{-1} HSA solution was titrated manually by successive additions of stock solution of Cafaminol, to span the drug concentration range, from 0 to 40 μmol L^{-1}. After each drug addition, the complex solution was left for 3 min, to reach equilibrium at the desired temperature; then fluorescence intensities were measured.

2.2.2. Synchronous spectroscopy

Synchronous fluorescence (SF) spectrometry is able to provide information on the molecular environment in the vicinity of the chromophore molecules. This technique has several advantages such as spectral bandwidth reduction, simplification of the emission spectra, contraction of the spectral range and avoiding different perturbing effects (Lloyd & Evett, 1977).

SF spectra were recorded by simultaneously scanning the emission and excitation monochromators, when $\Delta\lambda$ between excitation and emission wavelengths was set to 15 or 60 nm, giving characteristic information about the Tyr and Trp residues, respectively. Measurement of synchronous spectra was done by titrating 1 ml portion of 10 μmol L^{-1} HSA, with successive additions of Cafaminol to reach the maximum concentration of 40 μmol L^{-1}.

2.2.3. 3D fluorescence spectroscopy

Three-dimensional fluorescence spectroscopy is an effective and powerful method to provide comprehensive conformational and structural information about proteins. In this study, excitation and emission wavelengths were set between 200 and 500 nm, while other scanning parameters were the same as those for the fluorescence quenching spectra.

2.2.4. UV-visible absorption spectroscopy

Absorption spectra of HSA were recorded both in the absence and presence of Cafaminol, in the range of 250–400 nm, employing the carry spectrophotometer equipped with 1-cm quartz cell. HSA concentration was fixed at 20 μmol L^{-1}, while the Cafaminol concentration was varied from 0 to 40 μmol L^{-1}.

2.2.5. Circular dichroism (CD) measurement

CD is an optical technique to monitor the protein's conformational changes. In this study, CD spectra were recorded using Aviv Circular Dichroism Spectrometer Model-215, in the range of 190–260 nm, at room temperature under constant nitrogen flush rate of 30 l/min. Measurements were taken at constant 10 μmol L^{-1} HSA concentration, while Cafaminol was added gradually to cover the concentration range of 0 to 74 μmol L^{-1}.

2.2.6. Molecular dynamics simulation

MD simulation is the most comprehensive computational method that allows one to predict the time evolution of a molecular system of interacting particles. In this study, two separate MD simulations were performed on pure HSA and HSA-Cafaminol complex, respectively, in order to find the equilibrium structure of HSA at semi-physiological conditions and to analyze the conformational changes of HSA upon binding to Cafaminol.

In this respect, initial structure of HSA (PDB ID: 4k2c) was downloaded from the RCSB website and required topology and interaction parameters were created using the standard GROMOS9643a1 force field. The PRODRG 2.5 automated server (Schüttelkopf & Van Aalten, 2004), a tool for quickly generating topologies was employed to produce topology parameters for Cafaminol, within the framework of the GROMOS96-43a1 forcefield.

After insertion of protein in a cubic box of simple point charge (SPC) water molecules, the steepest descent algorithm was employed to run energy minimization, followed by the two short position restrained MD simulations, in NVT and NPT ensembles, each for 100 ps. The system was subjected to these equilibration steps, in order to reach to the specified temperature (310 K) and pressure (1 bar).

It should be mentioned that velocity verlet algorithm [40] was used for allocating initial velocities to atoms, based on the Maxwell distribution. Cutoff value for short range van der Waals interactions was set to 1.4 nm, while the Particle Mesh Ewald was employed to treat the long-range electrostatic interactions.

After NVT and NPT equilibration steps, the system was subjected to a 20 ns MD simulation (using leap-frog

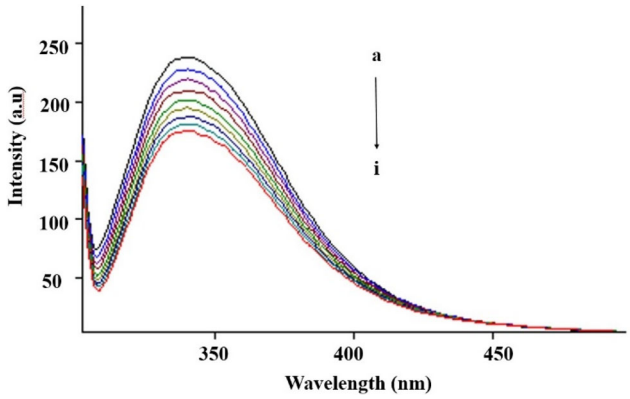

Figure 3. Conventional fluorescence spectra of HSA, at 289 K. HSA: 10 μmol L^{-1}; Cafaminol (a–i): 0–40 μmol L^{-1}.

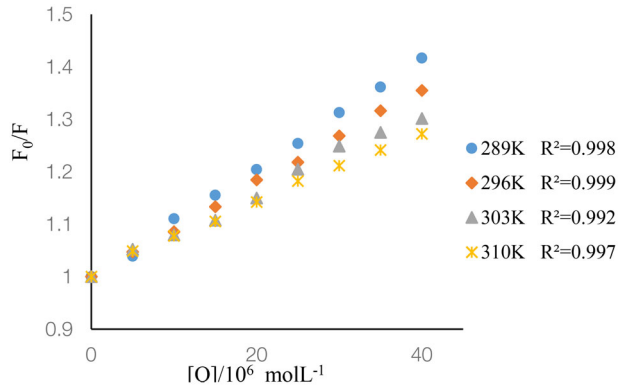

Figure 4. Stern-Volmer plots for the fluorescence quenching of HSA, at different temperatures. HSA: 10 µmol L^{-1}, Cafaminol: 0–40 µmol L^{-1}, pH = 7.4.

integrator), at 310 K, while the trajectory was analyzed by the Gromacs package tools. Above mentioned steps were repeated for the HSA-Cafaminol mixture, to assess the structural changes in HSA, induced by Cafaminol. All calculations and analyzes were performed using the Gromacs 5.1.4 simulation package.

2.2.7. Docking

Cafaminol's structure was generated by the Chemdraw ultra 8, and energy minimized in a two-step process. Energy minimization was first implemented by AM1, a semi-empirical method to ensure that the main structure is good enough for initiating the main energy minimization step, by the Guassian 09 software. In the next step, the Auto Dock Tools version 1.5.6 software (http://mgltools.scripps.edu) was used to prepare the docking input files, by Reading drug coordinates, adding necessary charges, merging non-polar hydrogens, and defining the rotatable bonds. Auto Dock Vina was then employed to dock drug molecule, into the equilibrated receptor (HSA) structure (obtained from the MD simulation). During the docking process, HSA structure was set rigid, while considering flexibility for the ligand, via genetic algorithm.

3. Results and discussion

3.1. Fluorescence quenching

Fluorescence quenching is a physicochemical process involved in molecular interaction between fluorophore and quencher, which lowers the intensity of emitted light from the fluorescent molecules. This phenomenon occurs due to a variety of events, such as excited state reactions, energy transfer, collisional quenching and ground state complex formation (Lakowicz, 2013).

There are two distinct mechanisms for the fluorescence quenching, namely dynamic and static. Dynamic (or collisional) quenching occurs due to the diffusive encounter between fluorophore (F) and quencher (Q); while on the other hand, static (or contact) quenching is mainly based on the formation of non-fluorescent (FQ) complex (Chen et al., 1990).

These two mechanisms are distinguished based on their responses to the temperature. Taking into account that higher temperatures give rise to larger diffusion coefficients, and the dependence of dynamic quenching on the diffusion, it is expected that bimolecular quenching constants increase with the increasing temperature. Contrarily, in static quenching, temperature increase leads to the decrease in complex stability, so lowers the quenching constant values (Hu et al., 2005).

In this study, HSA, acting as a fluorophore, has 1 tryptophan, 18 tyrosine and 32 phenylalanine residues. The intrinsic fluorescence of HSA comes mainly from tryptophan alone, because phenylalanine has a very low quantum yield, and the fluorescence of tyrosine is totally quenched if it is ionized or is near an amino group, a carboxyl group or a tryptophan residue (Sułkowska, 2002).

When studying HSA fluorescence, in order to prevent tyrosine from getting excited, normally an excitation of 295 nm is used. Figure 3 depicts the fluorescence quenching spectra of HAS, in the presence of different concentrations of Cafaminol (acting as a quencher). It is clear that the fluorescence intensity is decreased gradually with the increasing concentrations of Cafaminol, which in turn confirms the binding of Cafaminol to HSA.

The Stern-Volmer equation is often employed to determine the fluorescence quenching mechanism, induced by a ligand, here the Cafaminol.

$$\frac{F_0}{F} = 1 + K_{SV}[Q] \quad (1)$$

$$K_{SV} = k_q \tau_0 \quad (2)$$

where F_0 and F are the fluorescence intensities, respectively, in the absence and presence of the quencher. k_q is the bimolecular quenching rate constant, [Q] is the concentration of quencher, and K_{sv} is the Stern-Volmer quenching constant, providing a direct measure of the quenching efficiency.τ_0 is the average lifetime of the fluorophore (without quencher), where the fluorescence lifetime of biopolymers is about 10^{-8} s (Feng et al., 1998), so the values of k_{sv} are similar to k_q values, except for the difference in power.

Figure 4 represents the Stern-Volmer plots at different temperatures, which are linear, with the decreasing slopes against temperature, providing an evidence for the static

Table 1. Stern-Volmer quenching constants (K_{SV}), binding constants (K_b), binding sites (*n*) and Thermodynamic parameters.

		Quenching mechanism				Binding parameters		
T (K)	$K_{SV}\times10^3$ (M^{-1})	ΔG (kJ mol^{-1})	ΔH (kJ mol^{-1})	ΔS (J mol^{-1} K^{-1})	R^2	N	K_b ($\times10^3$ M^{-1})	R^2
289	10.46 ± 0.02	−24.64	−105.88	−282.34	0.99	1.10	28.44 ± 0.04	0.98
296	8.92 ± 0.02	−22.03			0.99	0.98	7.71 ± 0.04	0.99
303	7.70 ± 0.02	−19.76			0.99	0.89	2.59 ± 0.04	0.98
310	6.70 ± 0.02	−18.762			0.99	0.85	1.47 ± 0.04	0.99

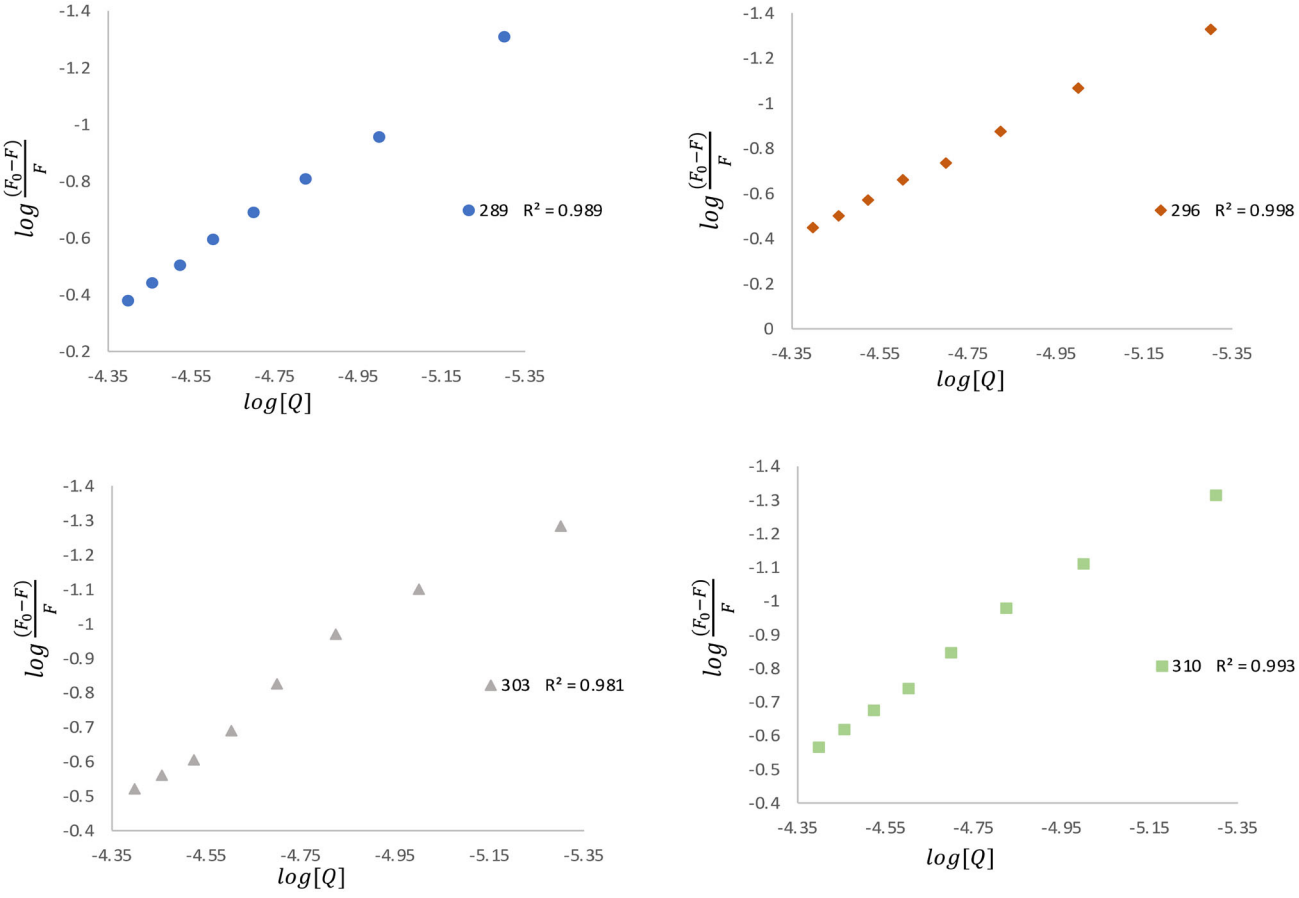

Figure 5. Double log plots (log $\frac{(F_0-F)}{F}$ vs. log [Q]) for HSA fluorescence quenching at different temperatures. HSA: 10 μmol L−1, Cafaminol: 0–40 μmol L−1, pH = 7.4

quenching mechanism. Table 1 reports the K_{sv} values (Stern-Volmer quenching constants), obtained from the slopes of Stern-Volmer plots, at different temperatures.

It should be mentioned that the maximum scatter collision quenching constant (k_q) for various quenchers of biopolymers, is about 2.00×10^{10} M^{-1} S^{-1} (Yuan et al., 2011). Here, the quenching constants of HSA induced by Cafaminol (reported in Table 1) are greater than 2.00×10^{10} M^{-1} S^{-1}, which is another proof that the quenching process occurs by the complex formation between HSA and drug.

For static quenching interaction, the binding constant and stoichiometry can be calculated using the following equation, if it is assumed that there are comparable and independent binding sites in the biomolecule (Lakowicz, 2013):

$$log\frac{(F_0-F)}{F} = logK_b + nlog[Q] \quad (3)$$

Again F and F_0 are the fluorescence intensities with and without quencher, respectively. K_b is the binding constant and *n* is the number of binding sites per albumin molecule, where a plot of log $(F_0-F)/F$ versus log [Q] is employed to determine K_b. Figure 5 depicts these double log plots, for the fluorescence quenching of HSA, at different temperatures. The correlation coefficients which are greater than 0.99 (reported in Table 1) show acceptable agreement between the HSA-Cafaminol interaction, and the site binding, underlying Eq. (3). K_b and *n* values, obtained from Eq. (3), are also reported in Table 1. *n* values were found to be approximately 1, meaning that HSA has only a single binding site for Cafaminol. In other words, regardless of the present number of Cafaminol molecules in solution, HSA is able to carry just one Cafaminol molecule.

According to the Table 1, K_b values for binding of Cafaminol to HSA are on the order of 10^3 M, showing the moderate binding affinity between these two molecules. This justification is based on the fact that high affinity binding constants of ligand-protein are in the range of 10^6–10^8 M (53). Such a moderate binding affinity is benefited for the efficient transport of drug, and its subsequent release, at the target site.

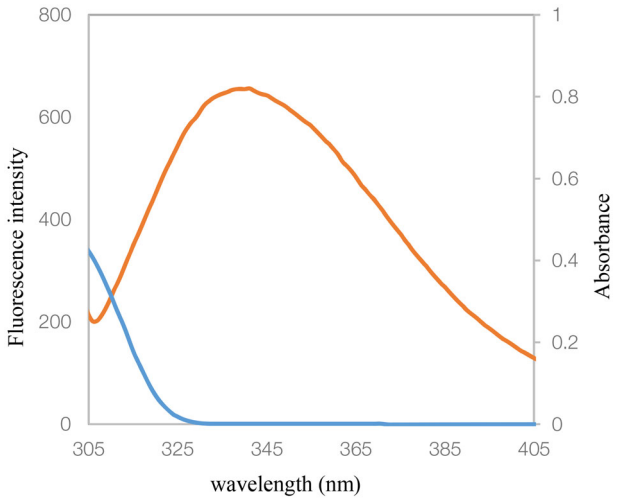

Figure 6. Overlap spectra of Cafaminol UV absorption spectrum and the fluorescence emission spectrum of HAS. [HSA] = 30×10^{-6} mol L^{-1}, [Cafaminol] = 30×10^{-6}mol L^{-1}.

In order to reduce the inner filter effect, all fluorescence intensities were corrected for absorption of the exciting light and reabsorption of emitted light, using the following relationship (Lakowicz, 2013; Rashidipour et al., 2016)

$$F_{cor} = F_{obse}^{(A_{ex}+A_{em})/2} \quad (4)$$

where F_{cor} and F_{obs} are, respectively, the corrected and observed fluorescence intensities. In addition, A_{ex} and A_{em} are the system absorptions at excitation and emission wavelengths, respectively.

3.2. Thermodynamic parameters and the binding constant

When a small molecule binds to a macromolecule, several types of non-covalent interactions such as Van der Waals forces, hydrogen bonding, electrostatic and hydrophobic interactions may occur. It is evident from Table 1 that temperature is an important parameter affecting the binding process, while the lower temperatures favor the stability of the HSA-Cafaminol complex. Therefore the temperature dependent thermodynamic parameters (free energy change, and the entropy and enthalpy changes) were analyzed in order to characterize the nature of main contributing forces to the HSA-drug complex formation (Ross & Subramanian, 1981).

Simultaneous $\Delta H > 0$ and $\Delta S > 0$ imply a hydrophobic association; while $\Delta H < 0$ and $\Delta S < 0$ confirm the existence of the van der Waals forces, or the formation of hydrogen bonding, and electrostatic forces are specified by $\Delta H < 0$ and $\Delta S > 0$ (Ross & Subramanian, 1981).

The enthalpy and entropy changes were determined, respectively, from the slope and the y-intercept of the van't Hoff equation.

$$lnK = -\frac{\Delta H}{RT} + \frac{\Delta S}{R} \quad (5)$$

The free energy change was later calculated using the following relationship:

$$\Delta G = -RTlnK \quad (6)$$

Here T is the temperature in Kelvin and R is the universal gas constant (8.31 J mol^{-1} K^{-1}). Examination of the Thermodynamic parameters (reported in Table 1) showed that Cafaminol-HSA complex formation is an exothermic and spontaneous process. On the other hand, negative ΔS and ΔH values indicated that van der Waals forces and hydrogen bonding play the dominant roles in the binding of Cafaminol to HSA. The binding process was found to be enthalpy driven, because the main contribution to the ΔG value was from ΔH, while the ΔS factor had smaller portion. It is known that enthalpy driven interactions favor hydrogen bonding in the low dielectric moieties like water, and Van der Waals interactions get into the game, directly duo to hydrophobic interactions (Kang et al., 2004; Ross & Subramanian, 1981).

3.3. Fluorescence resonance energy transfer (FRET) from HSA to Cafaminol

FRET is a non-destructive spectroscopic mechanism, describing energy transfer between two light-sensitive molecules. Energy may transfer from the donor, initially in its electronic excited state, to an acceptor through the non-radiative long range dipole-diploe interactions (Helms, 2018).

According to the FRET theory, the energy transfer will occur under the following three conditions: (I) Donor can produce fluorescence light, (II) Fluorescence emission spectrum of donor and UV-vis absorbance spectrum of acceptor have overlap and, (III) Distance between donor and acceptor is less than 8 nm (Szabo & Ostlund, 2012). Spectral overlap of the donor (HSA) and acceptor (Cafaminol) is shown in Figure 6.

The efficiency of energy transfer (E) is inversely proportional to the sixth power of the distance (r_0) between donor and acceptor, and the critical energy transfer distance (R_0). E is calculated through the following equation:

$$E = 1 - \frac{F}{F_0} = \frac{R_0^6}{R_0^6 + r_0^6} \quad (7)$$

where F and F_0, respectively, are the fluorescence intensities of HSA after the ligand addition, and free HSA.

R_0, the critical distance at 50% efficiency, is obtained from Eq. (8).

$$R_0^6 = 8.79 * 10^{-25} K^2 N^{-4} \phi J \quad (8)$$

Here, K^2 is the spatial orientation factor, related to the geometry of dipoles; N is the average refractive index of medium (in the wavelength range, where spectral overlap is significant); ϕ is the fluorescence quantum yield of the donor; and J is the overlap integral between the emission spectrum of donor and the absorbance spectrum of acceptor, given by:

$$J = \frac{\Sigma F_\lambda \varepsilon_\lambda \lambda^4 \Delta\lambda}{\Sigma F_\lambda \Delta\lambda} \quad (9)$$

where $F(\lambda)$ is the fluorescence intensity of donor and $\varepsilon(\lambda)$ is the molar absorption coefficient of the acceptor, both at wavelength λ.

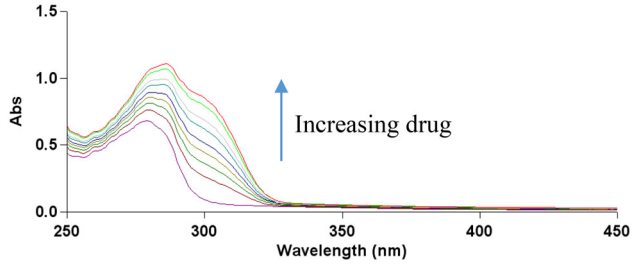

Figure 7. UV–vis spectra of HSA in the absence and presence of Cafaminol at room temperature and pH 7.4. [HSA] = 20×10^{-6}mol L^{-1}; [Cafaminol] = (0–40) $\times 10^{-6}$ mol L^{-1}.

In the present study for HSA-Cafaminol complex, $n = 1.36$ and $\phi = 0.07$ (Hu et al., 2005), so based on Eqs. (7)–(9), $J = 2.60 \times 10^{-14}$ cm^3 L mol^{-1}; $R_0 = 2.63$ nm, and the binding distance $r = 3.28$ nm. The value of binding distance (r), falling in the ($0.5\,R_0 < r < 1.5\,R_0$) range, confirms the occurrence of energy transfer from HSA to Cafaminol. On the other hand, r value is greater than R_0, which is another evidence for the static quenching mechanism (Shi et al., 2020).

3.4. UV-vis absorption spectra

UV–vis measurement is a simple and effective spectroscopic method to explore the structural changes and specify the complex formation. Native HSA spectra depicts two absorption peaks at 233 and 278 nm, respectively, due to the characteristic π–π^* transition of polypeptide backbone structure of C = O, and n–π^* transition of aromatic amino acids, i.e. Trp, Tyr and Phe (Shu et al., 2011).

It is well known that the dynamic quenching only affects the excited state of fluorophore, without changing the absorption spectra. In contrast, the complex formation in the ground state is able to change the absorption spectrum of the fluorophore (Lakowicz, 2013).

As shown in Figure 7, the UV absorption intensity of HSA was increased with the increasing amount of Cafaminol, while the maximum absorption slightly shifted towards the longer wavelengths. It should be mentioned that the UV-vis absorption spectra of the protein were obtained through subtracting the absorption contribution of free Cafaminol (Figure S4), from that of HSA-Cafaminol mixture.

These observations support the idea of complex formation between HSA and Cafaminol, accompanied by the induced changes in HSA structure, which provide another proof for the static quenching mechanism.

3.5. Circular dichroism (CD) spectra analysis

Due to the remarkable sensitivity of CD spectra in UV region to the backbone conformation of proteins, this technique is employed to assess alterations in the secondary and tertiary structures of HSA protein. In the CD diagram of free HSA, two negative bands at 208–209 and 222–223 nm (in the far ultra-violet region) are contributed to the π–π^* and n–π^* transfers, characterizing the albumin's alpha-helical structure.

As seen in Figure 8, with the increasing concentrations of Cafaminol, the CD spectra of HSA show decreasing band

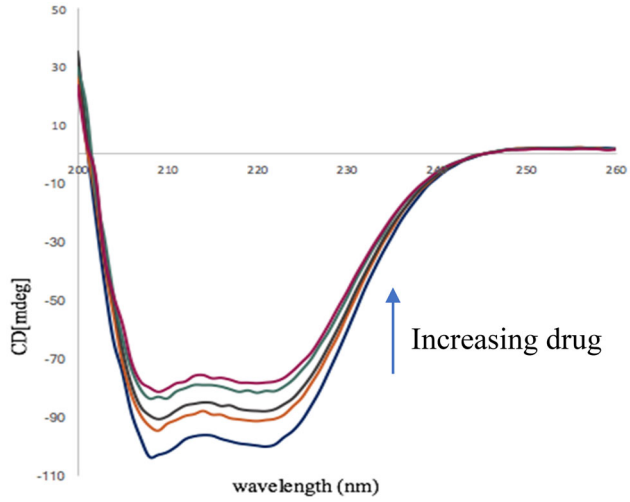

Figure 8. CD spectra of HSA in the presence of various concentrations of Cafaminol ($T = 298$ K). C [HSA] = 10×10^{-6}mol L^{-1}, and C [Cafaminol] = 0–74.07×10^{-6} mol L^{-1}.

intensities at all wavelengths of the far-UV, without any significant shifts of the peak positions. This observation reveals the peptide strand unfolding and the decrease of α-helical content of HSA. It should be mentioned that the main spectra shape of HSA remains similar in the presence and absence of Cafaminol, showing that the structure of HSA is predominantly α-helical.

The CD result can be expressed as MRE (mean residue ellipticity) in deg cm^2 $dmol^{-1}$, according to the following equation (Chen et al., 1972):

$$MRE = \frac{ObservedCD(mdegree)}{Cpnl \times 10} \tag{10}$$

where C_p, n and l are the molar concentration of the protein (HSA), number of amino acid residues (585 for HSA) and the path-length of the cell (1 cm), respectively. The alpha-helix contents of free and combined HSA were calculated from the MRE values at 208 nm, using Eq. (11) (Khan et al., 2008).

$$\propto -Helix(\%) = \frac{MRE_{208} - 4000}{33000 - 4000} \times 100 \tag{11}$$

Calculated results showed the decrease of alpha-helicity in the secondary structure of HSA from 75% to 60.91% (with the increasing concentrations of Cafaminol), which is in acceptable agreement with the CD spectra.

3.6. Synchronous fluorescence

Complementary to the CD measurements, synchronous fluorescence spectra of HSA, with various amounts of Cafaminol, were carried out to assess the micro environmental changes in a vicinity of the chromophore molecules. When the excitation and emission monochromators of a fluorimeter are scanned simultaneously, the synchronous fluorescence spectra are obtained. According to Miller (1979), the fluorescence spectra of HSA with $\Delta\lambda$ of 60 and 15 nm, are characteristics of tryptophan and tyrosine residues, respectively.

Figure 9 shows the effect of Cafaminol on the synchronous fluorescence spectra of HSA. It is clear that the intensity

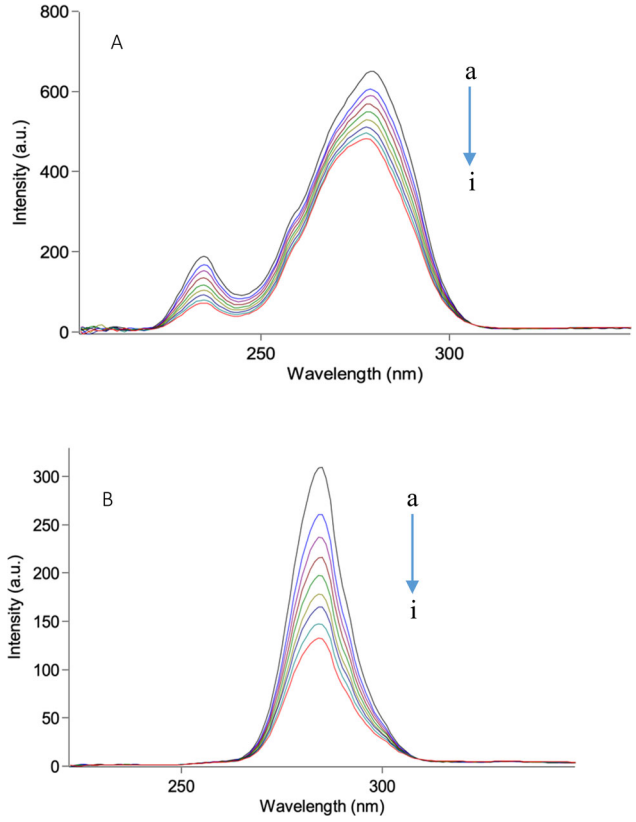

Figure 9. The synchronous fluorescence spectra of HSA-Cafaminol. (A) $\Delta\lambda = 60$ nm; (B) $\Delta\lambda = 15$ nm. C [HSA] $= 10 \times 10^{-6}$ mol L^{-1} while concentrations of Cafaminol were 0.0–40.0 $\times 10^{-6}$ mol L^{-1} (a–i).

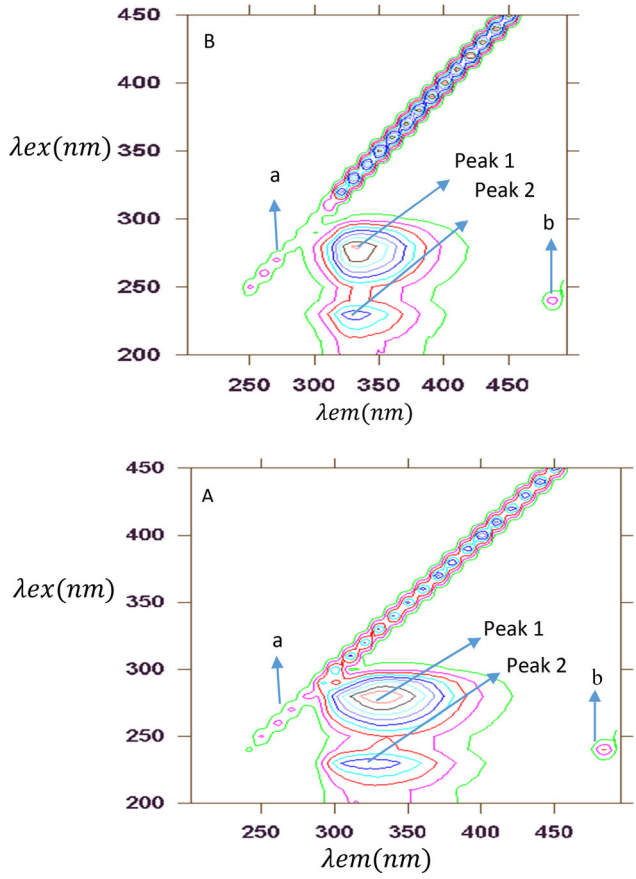

Figure 10. Three-dimensional fluorescence contour diagrams of (A) HSA, (B) HSA-Cafaminol, at $T = 298$ K and pH = 7.4. [HSA] = 30 μM; [Cafaminol] = 30 μM.

of tryptophan residue is greater than that of tyrosine residues, indicating that tryptophan contributes strongly to the quenching of intrinsic fluorescence of HSA.

Observing a small blue shift (1.07 nm and 1.1 nm, respectively, for $\Delta\lambda = 15$ nm and $\Delta\lambda = 60$ nm) in both A and B spectra implies an increase in the hydrophobicity and decrease in the polarity around the tryptophan and tyrosine residues (Hu et al., 2005).

3.7. 3D fluorescence spectra

The three dimensional fluorescence spectra depict the microenvironmental changes around the protein fluorophores (Tyr & Trp). Successively using the excitation and emission monochromators makes it possible to measure emission spectra for different excitation wavelengths, with a constant step. The emission-excitation matrices have two dimensions, excitation wavelengths (λ_{ex}) and emission wavelengths (λ_{em}), and provide a type of fluorescence map of all the fluorophores (Locquet et al., 2006).

The contour map provides bird's eye view of 3D fluorescence spectra. Shown in Figure 10, peaks a and b are, respectively, the Rayleigh scattering peak ($\lambda_{ex} = \lambda_{em}$) and the second-order scattering peak ($\lambda_{ex} = 2\lambda_{em}$), due to the π–π^* transition of the characteristic polypeptide backbone structure C = O of HSA (Pan et al., 2011).

Two other peaks are also observed in 3D fluorescence spectra of protein, Peak 1 indicates the spectral characteristics of Trp and Tyr residues, while peak 2 is due to excitation of higher excited electronic states of the aromatic residues, present in the protein (Bortolotti et al., 2016).

It is clear that both fluorescence peaks (1 and 2) of HSA have been quenched in response to the Cafaminol addition, which is another proof for the binding of Cafaminol to HSA that leads to the change in protein's conformation. Close look at the 3D fluorescence spectra of pure HSA, and HSA-Cafaminol mixture (Figure 10) shows that changes in the fluorescence intensity of peaks 1 & 2 are, respectively, 84.55 and 43.38 a.u. This conformational change is along with unfolding some hydrophobic regions of HSA, which were buried before.

3.8. Molecular dynamics simulation

At the end of 20 ns MD simulation, some analyzes were performed on the trajectory file of pure HSA, to ensure that it has reached to the equilibrium state in a semi-physiological condition. Simultaneous analyzes were also implemented on HSA-Cafaminol simulated complex, to assess the induced structural and conformational changes on HSA molecule, due to the complex formation.

In the three following subsections, analysis of root mean square deviation (RMSD), radius of gyration (Rg) and root mean square fluctuations (RMSF) for both pure HSA and HSA-Cafaminol complex will be discussed.

3.8.1. Root mean square deviation (RMSD)

Root mean square deviation is a common method to determine the stability of a system (e.g. backbone of a protein) and provides quantitative measure of the similarity between two superimposed atomic coordinates. The value of RMSD between two sets of coordinates, from two time points of simulation trajectory, is a measure of how much the protein conformation has been changed.

This property is calculated through the following equation, where N is the number of atoms, and u_i and ν_i are the initial and final atomic points, respectively.

$$RMSD(t) = \sqrt{\frac{1}{N}\sum_{i=1}^{N}(u_i - \nu_i)} \tag{12}$$

As depicted in Figure 11(A), the RMSD value of C-α atoms of free HSA, first rises from 0.2 to about 0.4 nm, and then oscillates around the average value of 0.43 nm, mainly after 9 ns of the simulation time. This evidence confirms the establishment of quasi-equilibrium state for HSA.

In the case of HSA-Cafaminol complex, backbone RMSD shows lower oscillations and increases from 0.13 to about 0.28 nm, where it remains almost constant afterwards. This is an indication of higher protein's backbone stability, in a complex form.

3.8.2. Radius of gyration (Rg)

Radius of gyration which is another parameter for describing the equilibrium conformation of protein is an indicator of its structure compactness. A stably folded protein will maintain a relatively steady value of Rg, but if a protein unfolds, its Rg will change over time (Lobanov et al., 2008b)

Rg is calculated in two steps: First, the center of mass (R_C) coordinates are determined using Eq. (13), while the hydrogen atoms are neglected:

$$\sum m_i(r_i - R_C) = 0 \tag{13}$$

m_i and r_i are the mass and position vector of the ith atom, respectively.

Then, considering the atoms as points in a 3D space, Rg is obtained from:

$$R_g^2 = \sum m_i(r_i - R_C)^2/M \tag{14}$$

where M is the total mass of protein atoms (Lobanov et al., 2008a).

As indicated in Figure 11(B), Rg values for both HSA and HSA-Cafaminol complex reach a plateau after about 9 ns, which is another clue for achieving the quasi equilibrium state. Lower Rg values for HSA in a complex form is due to the conformational changes induced by the Cafaminol, leading to a little more compact structure.

3.8.3. Root mean square fluctuations (RMSF)

Root mean square fluctuations (RMSF) is a numerical measurement of individual atom or residue flexibility (dynamism), or how much it moves (fluctuates) during a simulation. Therefore one can determine which aminoacid in a protein contributes the most to a molecular motion. In this study, RMSF was calculated using Eq. (15), to get an estimation of the ith particle's position from its reference position (Moeinpour et al., 2016).

$$RMSF_i = \left[\frac{1}{T}\sum_{t_j=1}^{T}||r_i(t_j) - r_i^{ref}||^2\right]^{1/2} \tag{15}$$

where T is the time over which one wants to take average and r_i^{ref} is the reference position of particle i. Generally this reference position will be the time-averaged position of the same particle i, i.e. $r_i^{ref} = r_i$.

Inspection of Figure 11(C) reveals that most regions of protein are stabilized after binding to Cafaminol, showing lower RMSF values for protein atoms. Greater fluctuations of the protein's terminal residues in both free and complex form are due to their ability to move more freely.

3.8.4. Molecular docking

In general, spectroscopic studies cannot provide information on binding at the atomic level, so molecular modeling studies are employed as complementary approach to obtain microscopic information on the interactions between small molecules and receptor. Molecular docking is able to predict the preferred orientation and binding position of one molecule to the second, in order to form a stable complex.

In the present study, docking of Cafaminol into the equilibrated structure of HSA (obtained from MD simulation at 310 K) was implemented with the Auto Dock vina (Trott & Olson, 2010). This program needs both the receptor and ligand files in the PDBQT format, so, the 3D coordinate file of receptor (HSA) was saved into this format. In order to obtain the energy minimized structure of Cafaminol, Gaussian 09 was employed at the B3LYP level of theory, along with the 6–31 ++ g(2d) basis set (Frisch et al., 2003). Center of the docking grid was set to $x = 49.34$, $y = 53.25$ and $z = 66.46$, with the maximum spacing of 1 Å, where the grid-size was kept at $90 \times 76 \times 90$ Å, to cover the entire receptor molecule.

Auto Dock vina yielded nine most stable conformations, arranged in the order of increasing binding energies, while the conformation with the lowest binding energy was chosen for further analysis. The best energy-ranked result of the interaction between Cafaminol and HSA in all runs of docking procedure is shown in Figure 12.

In addition, docking results indicated that Cafaminol interacts with HSA with a binding energy (ΔG) of -6.5 kcal mol^{-1}, while the fluorescence data revealed that Cafaminol prefers to fit in the area between sub-domains IIA and IIIB, with ΔG of -4.48 kcal mol^{-1}. In fact, our in silico obtained results are in acceptable accordance with our experimental findings.

Later, the LIGPLOT (A program for automatically plotting protein ligand interactions) (Wallace et al., 1995) was employed to analyze the HSA and Cafaminol interactions. This program was used to specify the interactions mediated by hydrogen bonds and hydrophobic contacts (Figure 12B). Hydrogen bonds are indicated by dashed lines between the atoms involved, while hydrophobic contacts are represented

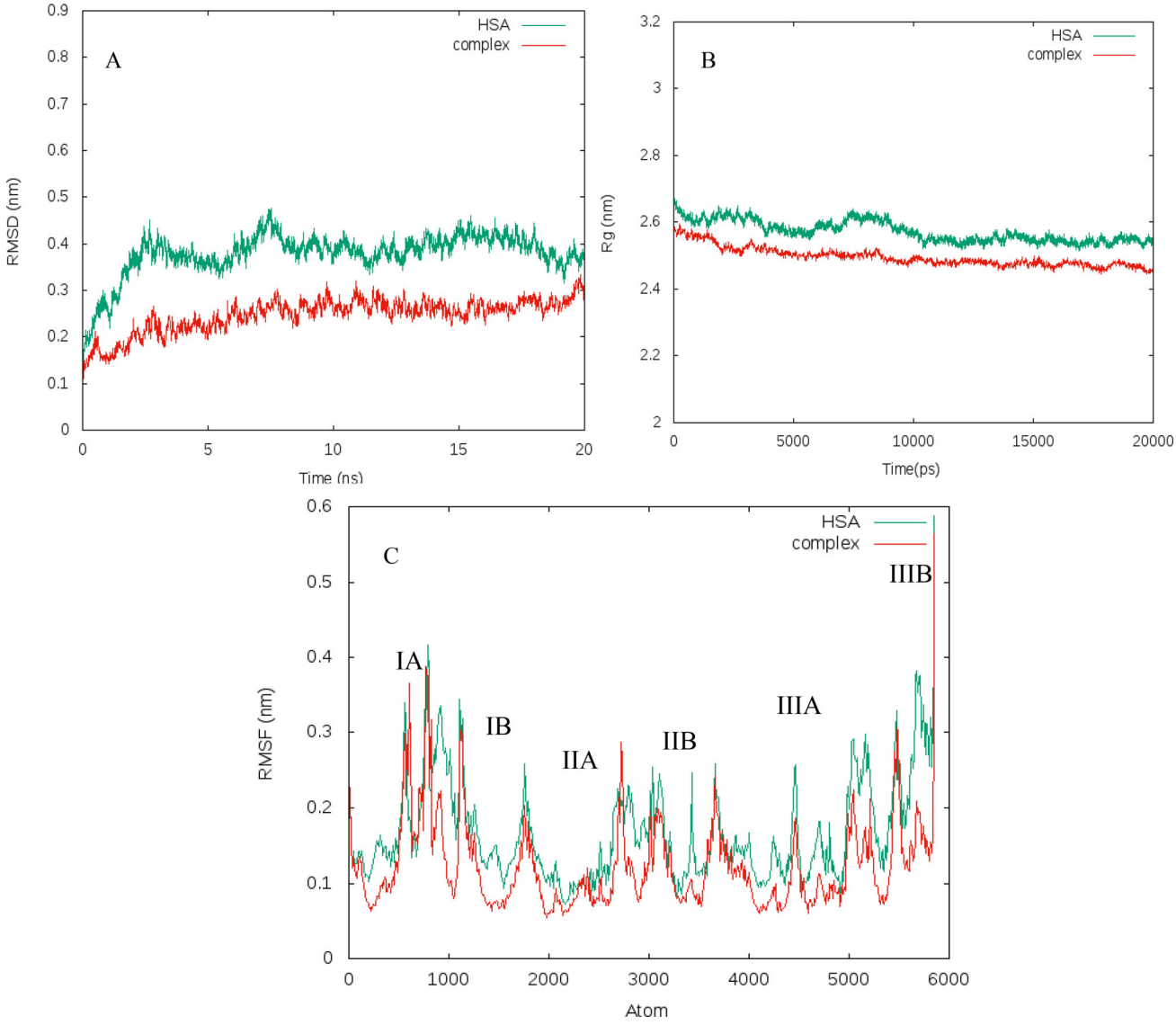

Figure 11. (A) RMSD of the HSA backbone in the presence and absence of Cafaminol, at 310 K. (B) Time evolution of the radius of gyration (Rg) during 20 ns of MD simulation for HSA and HSA-Cafaminol complex. (C) Root mean square fluctuations over atoms for HSA, in both free and complex form.

by an arc with spokes, radiating towards the ligand atoms they contact. Contacted atoms are shown with spokes radiating back.

Docking results showed that Cafaminol mainly interacts with HSA, through hydrogen bonding, which agrees well with the thermodynamic analysis outcome.

As shown in Figure 12, interaction of Cafaminol and HSA occurs in the area between sub-domains IIA and IIIB. Hydrogen bonds decrease the hydrophilicity, increase the hydrophobicity, and thus stabilize the HSA-Cafaminol complex.

4. Conclusion

Since albumin serves as a drug carrier, studying its interaction with different drugs is of importance in pharmacy, pharmacology and biochemistry. In the present study, the interaction of Cafaminol with the human serum albumin (HSA) was investigated through the various molecular spectroscopy methods, and molecular dynamics and docking simulations.

In total, it was determined that Cafaminol binds to the site I (Between sub-domains IIA and IIIB) of HSA, in an exothermic and enthalpy driven process.

Analysis of the Stern-Volmer plots revealed that Cafaminol quenches the fluorescence of HSA through the static quenching mechanism, due to the drug-protein complex formation. UV-Visible absorption spectra of HSA showed an obvious intensity increase, along with a slight red shift, due to the Cafaminol addition. These findings support the idea of Cafaminol-HSA complex formation, accompanied by the induced microenvironmental perturbations around the protein's chromophore.

Analysis of the circular dichroism (CD) spectra of HSA in both free and complex forms demonstrated the decrease of protein's α-helical content, due to the complex formation.

Both negative ΔH and ΔS values confirmed that the van der Waals and hydrogen bonding interactions stabilize the Cafaminol in the HSA binding domain. Moderate binding

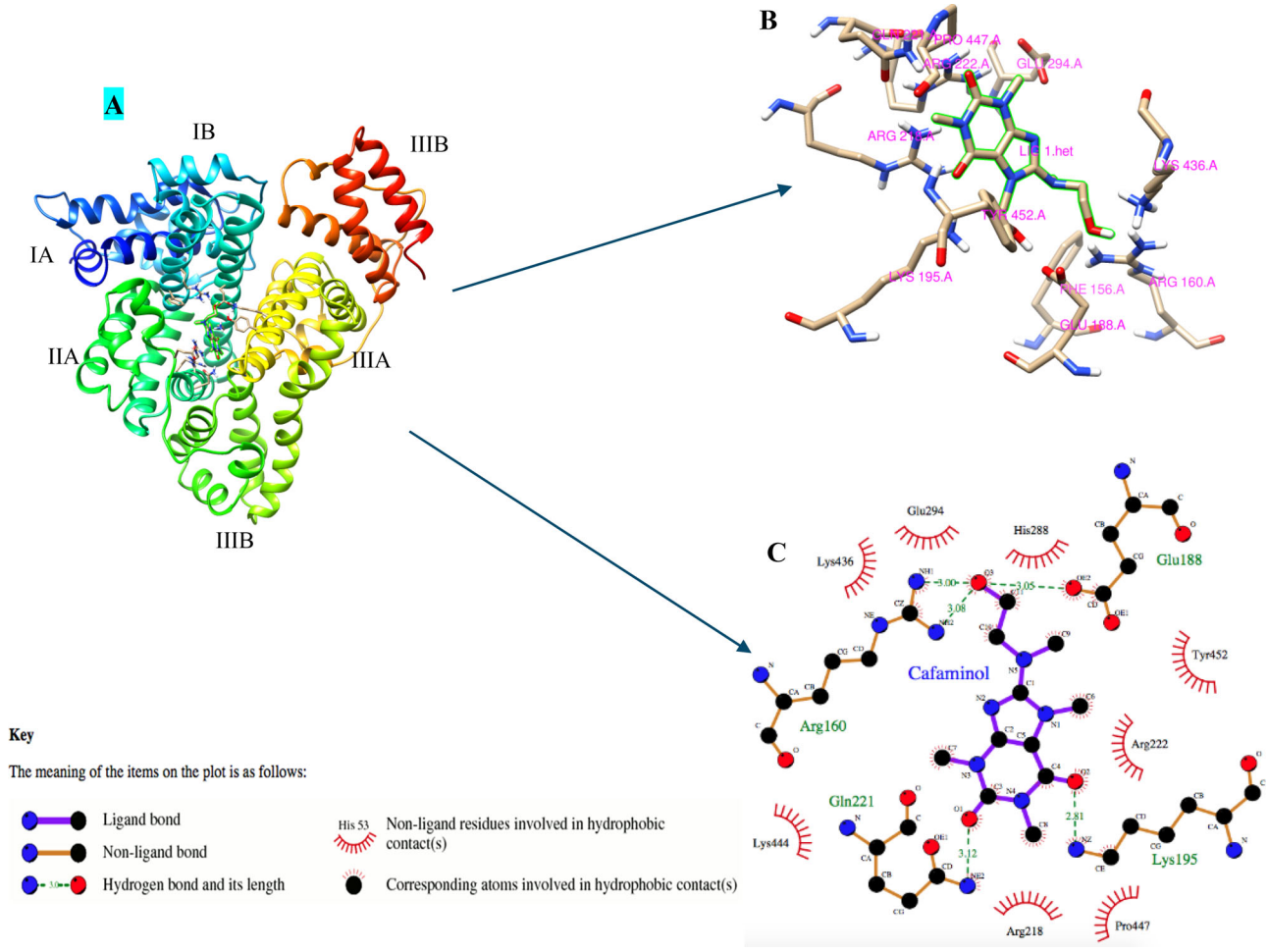

Figure 12. (A) Molecular docking pose of Cafaminol in HSA. (B) Cafaminol docked in the binding pocket of HSA. (C) Two-dimensional schematic representation of hydrogen bonding and hydrophobic interactions. Figure was plotted using the program LIGPLOT.

affinity between Cafaminol and HSA is benefited for the efficient transport of drug, and its subsequent release, at the target site. Overall results of molecular dynamics and docking simulations indicated the binding site of Cafaminol and made it possible to designate the main aminoacids involved in the drug-protein interactions.

References

Alavianmehr, M. M., Yousefi, R., Keshavarz, F., & Mohammad-Aghaie, D. (2014). Probing the binding of thioTEPA to human serum albumin using spectroscopic and molecular simulation approaches. *Canadian Journal of Chemistry*, *92*(11), 1066–1073. https://doi.org/10.1139/cjc-2013-0571

Bortolotti, A., Wong, Y. H., Korsholm, S. S., Bahring, N. H. B., Bobone, S., Tayyab, S., van de Weert, M., & Stella, L. (2016). On the purported "backbone fluorescence". *RSC Advances*, *6*(114), 112870–112876. in https://doi.org/10.1039/C6RA23426G

Bos, O. J., Fischer, M. J., Wilting, J., & Janssen, L. H. (1988). Drug-binding and other physicochemical properties of a large tryptic and a large peptic fragment of human serum albumin. *Biochimica et Biophysica Acta (BBA)*, *953*, 37–47. https://doi.org/10.1016/0167-4838(88)90007-6

Bos, O. J., Remijn, J. P., Fischer, M. J., Wilting, J., & Janssen, L. H. (1988). Location and characterization of the warfarin binding site of human serum albumin: A comparative study of two large fragments. *Biochemical Pharmacology*, *37*(20), 3905–3909. https://doi.org/10.1016/0006-2952(88)90072-X

Chen, G. Z., Huang, X. Z., Xu, J. G., Zheng, Z. Z., & Wang, Z. B. (1990). *The methods of fluorescence analysis* (2nd ed., pp. 112-145). Beijing: Science Press.

Chen, Y.-H., Yang, J. T., & Martinez, H. M. (1972). Determination of the secondary structures of proteins by circular dichroism and optical rotatory dispersion. *Biochemistry*, *11*(22), 4120–4131. https://doi.org/10.1021/bi00772a015

Du, X., Li, Y., Xia, Y.-L., Ai, S.-M., Liang, J., Sang, P., Ji, X.-L., & Liu, S.-Q. (2016). Insights into protein–ligand interactions: Mechanisms, models, and methods. *International Journal of Molecular Sciences*, *17*(2), 144. https://doi.org/10.3390/ijms17020144

Feng, X.-Z., Lin, Z., Yang, L.-J., Wang, C., & Bai, C.-l. (1998). Investigation of the interaction between acridine orange and bovine serum albumin. *Talanta*, *47*(5), 1223–1229. https://doi.org/10.1016/S0039-9140(98)00198-2

M. J. Frisch, G. W. Trucks, H. B. Schlegel, G. E. Scuseria, M. A. Robb, J. R. Cheeseman, G. Scalmani, V. Barone, G. A. Petersson, H. Nakatsuji, X. Li, M. Caricato, A. V. Marenich, J. Bloino, B. G. Janesko, R. Gomperts, B. Mennucci, H. P. Hratchian, J. V. Ortiz, … & D. J. Fox (2003). *Gaussian, revision B.* Gaussian Inc.

Helms, V. (2018). *Principles of computational cell biology: From protein complexes to cellular networks*. John Wiley & Sons.

Hu, Y.-J., Liu, Y., Pi, Z.-B., & Qu, S.-S. (2005). Interaction of cromolyn sodium with human serum albumin: A fluorescence quenching study. *Bioorganic & Medicinal Chemistry*, *13*(24), 6609–6614. https://doi.org/10.1016/j.bmc.2005.07.039

Hu, Y.-J., Liu, Y., Zhang, L.-X., Zhao, R.-M., & Qu, S.-S. (2005). Studies of interaction between colchicine and bovine serum albumin by fluorescence quenching method. *Journal of Molecular Structure*, *750*(1–3), 174–178. https://doi.org/10.1016/j.molstruc.2005.04.032

Hu, Y.-J., Liu, Y., Zhao, R.-M., & Qu, S.-S. (2005). Interaction of colchicine with human serum albumin investigated by spectroscopic methods. *International Journal of Biological Macromolecules*, *37*(3), 122–126. https://doi.org/10.1016/j.ijbiomac.2005.09.007

Kang, J., Liu, Y., Xie, M.-X., Li, S., Jiang, M., & Wang, Y.-D. (2004). Interactions of human serum albumin with chlorogenic acid and ferulic acid. *Biochimica et Biophysica Acta*, *1674*(2), 205–214. https://doi.org/10.1016/j.bbagen.2004.06.021

Keshavarz, F., Alavianmehr, M. M., & Yousefi, R. (2013). Molecular interaction of benzalkonium Ibuprofenate and its discrete ingredients with human serum albumin. *Physical Chemistry Research*, *1*(2), 111–116.

Khan, S. N., Islam, B., Yennamalli, R., Sultan, A., Subbarao, N., & Khan, A. U. (2008). Interaction of mitoxantrone with human serum albumin: Spectroscopic and molecular modeling studies. *European Journal of Pharmaceutical Sciences*, *35*(5), 371–382. https://doi.org/10.1016/j.ejps.2008.07.010

Lakowicz, J. R. (2013). *Principles of fluorescence spectroscopy*. Springer Science & Business Media.

Lloyd, J., & Evett, I. (1977). Prediction of peak wavelengths and intensities in synchronously excited fluorescence emission spectra. *Analytical Chemistry*, *49*(12), 1710–1715. https://doi.org/10.1021/ac50020a020

Lobanov, M. Y., Bogatyreva, N., & Galzitskaya, O. (2008a). Radius of gyration as an indicator of protein structure compactness. *Molecular Biology*, *42*(4), 623–628. https://doi.org/10.1134/S0026893308040195

Lobanov, M., Bogatyreva, N., & Galzitskaia, O. (2008b). Radius of gyration is indicator of compactness of protein structure. *Molekuliarnaia Biologiia*, *42*(4), 701–706.

Locquet, N., Aït-Kaddour, A., & Cordella, C. B. (2006). 3D fluorescence spectroscopy and its applications. In *Encyclopedia of analytical chemistry: Applications, theory and instrumentation* (pp. 1-39). Wiley Online Library.

Miller, J. (1979). Recent advances in molecular luminescence analysis. *Proceedings of the Analytical Division of the Chemical Society*, *16*, 203–208.

Moeinpour, F., Mohseni-Shahri, F. S., Malaekeh-Nikouei, B., & Nassirli, H. (2016). Investigation into the interaction of losartan with human serum albumin and glycated human serum albumin by spectroscopic and molecular dynamics simulation techniques: A comparison study. *Chemico-Biological Interactions*, *257*, 4–13. https://doi.org/10.1016/j.cbi.2016.07.025

Mohammad-Aghaie, D., Soltani Rad, N., Yousefi, R., Parvizi, N., Behrouz, S., & Alavianmehr, M. M. (2019). Probing the binding of valacyclovir hydrochloride to the human serum albumin. *Physical Chemistry Research*, *7*(4), 751–764.

Mokaberi, P., Babayan-Mashhadi, F., Amiri Tehrani Zadeh, Z., Saberi, M. R., & Chamani, J. (2020). Analysis of the interaction behavior between Nano-Curcumin and two human serum proteins: Combining spectroscopy and molecular stimulation to understand protein-protein interaction. *Journal of Biomolecular Structure and Dynamics*, 1–20. https://doi.org/10.1080/07391102.2020.1766570

Pan, X., Qin, P., Liu, R., & Wang, J. (2011). Characterizing the interaction between tartrazine and two serum albumins by a hybrid spectroscopic approach. *Journal of Agricultural and Food Chemistry*, *59*(12), 6650–6656. https://doi.org/10.1021/jf200907x

Peters Jr., T. (1995). *All about albumin: Biochemistry, genetics, and medical applications*. Academic press.

Poursoleiman, A., Karimi-Jafari, M. H., Zolmajd-Haghighi, Z., Bagheri, M., Haertlé, T., Behbehani, G. R., Ghasemi, A., Stroylova, Y. Y., Muronetz, V. I., & Saboury, A. A. (2019). Polymyxins interaction to the human serum albumin: A thermodynamic and computational study. *Spectrochimica Acta Part A*, *217*, 155–163. https://doi.org/10.1016/j.saa.2019.03.077

Rashidipour, S., Naeeminejad, S., & Chamani, J. (2016). Study of the interaction between DNP and DIDS with human hemoglobin as binary and ternary systems: Spectroscopic and molecular modeling investigation. *Journal of Biomolecular Structure & Dynamics*, *34*(1), 57–77. https://doi.org/10.1080/07391102.2015.1009946

Rogowski, M., & Chodynicki, S. (1985). Use of the preparation Cafaminol in the treatment of acute rhinitis. *Wiadomosci Lekarskie (Warsaw, Poland: 1960)*, *38*(20), 1437.

Ross, P. D., & Subramanian, S. (1981). Thermodynamics of protein association reactions: Forces contributing to stability. *Biochemistry*, *20*(11), 3096–3102. https://doi.org/10.1021/bi00514a017

Schüttelkopf, A. W., & Van Aalten, D. M. (2004). PRODRG: A tool for high-throughput crystallography of protein–ligand complexes. *Acta Crystallographica Section D Biological Crystallography*, *60*(8), 1355–1363. https://doi.org/10.1107/S0907444904011679

Seedher, N., & Bhatia, S. (2006). Interaction of non-steroidal anti-inflammatory drugs, etoricoxib and parecoxib sodium, with human serum albumin studied by fluorescence spectroscopy. *Drug Metabolism and Drug Interactions*, *22*(1), 25–46. https://doi.org/10.1515/dmdi.2006.22.1.25

Shahsavani, M. B., Ahmadi, S., Aseman, M. D., Nabavizadeh, S. M., Alavianmehr, M. M., & Yousefi, R. (2016). Comparative study on the interaction of two binuclear Pt (II) complexes with human serum albumin: Spectroscopic and docking simulation assessments. *Journal of Photochemistry and Photobiology B, Biology*, *164*, 323–334. https://doi.org/10.1016/j.jphotobiol.2016.09.035

Shi, W., Dong, S., & Hu, J. (2020). Neotectonics around the Ordos Block, North China: A review and new insights. *Earth-Science Reviews*, *200*, 102969. https://doi.org/10.1016/j.earscirev.2019.102969

Shu, Y., Liu, M., Chen, S., Chen, X., & Wang, J. (2011). New insight into molecular interactions of imidazolium ionic liquids with bovine serum albumin. *The Journal of Physical Chemistry B*, *115*(42), 12306–12314. https://doi.org/10.1021/jp2071925

Sohrabi, T., Hosseinzadeh, M., Beigoli, S., Saberi, M. R., & Chamani, J. (2018). Probing the binding of lomefloxacin to a calf thymus DNA-histone H1 complex by multi-spectroscopic and molecular modeling techniques. *Journal of Molecular Liquids*, *256*, 127–138. https://doi.org/10.1016/j.molliq.2018.02.031

Śpiewak, K., Stochel, G., & Brindell, M. (2015). Influence of redox activation of NAMI-A on affinity to serum proteins: Transferrin and albumin. *Journal of Coordination Chemistry*, *68*(17–18), 3181–3192. https://doi.org/10.1080/00958972.2015.1067692

Sugio, S., Kashima, A., Mochizuki, S., Noda, M., & Kobayashi, K. (1999). Crystal structure of human serum albumin at 2.5 A resolution. *Protein Engineering*, *12*(6), 439–446. https://doi.org/10.1093/protein/12.6.439

Sułkowska, A. (2002). Interaction of drugs with bovine and human serum albumin. *Journal of Molecular Structure*, *614*(1–3), 227–232. https://doi.org/10.1016/S0022-2860(02)00256-9

Szabo, A., & Ostlund, N. S. (2012). *Modern quantum chemistry: Introduction to advanced electronic structure theory*. Courier Corporation.

Trott, O., & Olson, A. J. (2010). AutoDock Vina: Improving the speed and accuracy of docking with a new scoring function, efficient optimization, and multithreading. *Journal of Computational Chemistry*, *31*(2), 455–461. https://doi.org/10.1002/jcc.21334

Wallace, A. C., Laskowski, R. A., & Thornton, J. M. (1995). LIGPLOT: A program to generate schematic diagrams of protein-ligand interactions. *Protein Engineering*, *8*(2), 127–134. https://doi.org/10.1093/protein/8.2.127

Yuan, D., Shen, Z. L., Liu, R. T., Wei, P. H., & Gao, C. Z. (2011). Study on the interaction of Nd^{3+} with human serum albumin at molecular level. *Journal of the Chinese Chemical Society*, *58*(4), 568–574. https://doi.org/10.1002/jccs.201190022